ELSEVIER

Development and application of wall-function treatments for turbulent forced and mixed convection flows

T.J. Craft*, S.E. Gant, A.V. Gerasimov, H. Iacovides, B.E. Launder

School of Mechanical, Aerospace & Civil Engineering, The University of Manchester, Manchester M60 1QD, UK

Abstract

CFD calculations of turbulent flow near smooth walls generally employ one of two broad strategies to resolve the very influential, complex, but thin near-wall viscosity-affected sub-layer. One approach uses a fine numerical mesh and a turbulence model incorporating viscous influences; the other employs "wall functions"—formulae that attempt to account for the overall resistance of the sublayer to momentum and heat transport. The latter requires only a fraction of the computational effort of the former and is thus strongly favoured for industrial calculations. However, the wall-function performance is often poor, partly because of inappropriate implementations and partly because the schemes themselves have inherent limitations.

The present paper reviews the evolution of wall-function strategies. Attention is then given to two new schemes developed by the authors, one based on an analytical treatment and the other on a numerical resolution of the near-wall sub-layer. Several applications are shown of mixed and forced convection.
© 2005 The Japan Society of Fluid Mechanics and Elsevier B.V. All rights reserved.

Keywords: Wall functions; Near-wall turbulence modelling; Heat transfer

1. Introduction

In most practical problems of convective heat transport to or from a rigid surface, the flow in the vicinity of the body is in turbulent motion. However, at the solid–fluid interface itself, the no-slip boundary

_____

* Corresponding author. Fax: +44 161 306 3723.

  E-mail address: tim.craft@manchester.ac.uk (T.J. Craft).

condition ensures that turbulent velocity fluctuations vanish. Thus, at the wall, diffusive transport of heat and momentum in the fluid is precisely expressible by the laws applicable to laminar flow. Indeed, because the turbulent shear stress, and often the turbulent heat flux, can, by continuity, increase only as the cube of the distance from the wall, there is a thin but very important sub-layer immediately adjacent to the solid surface where the transport of heat and momentum is predominantly by molecular diffusion. Further from the wall, again by virtue of the cubic variation, there is a very rapid changeover to a state where turbulent transport dominates, a condition that normally prevails over the remainder of the flow. This thin sub-layer and the adjacent transition region extending to the fully turbulent regime—what collectively we shall term the viscosity-affected sub-layer (VSL)—is the subject of the present paper. In particular, we are concerned with how one can accurately model the flow in this region in a form suitable for use in CFD software.

However, accuracy is not the only criterion. The VSL, as implied above, is a region where effective transport properties change at a rate typically two or more orders of magnitude faster than elsewhere in the flow. So, if one adopts the same numerical strategy, a very much finer mesh is required. Consequently, while the VSL typically occupies only around 1% of the flow, resolving that region can require between 3 and 300 times as much computing time (depending upon the flow problem, the mathematical model of turbulence and the type of CFD solver adopted) as would be required if the mesh density could be kept comparable with that in the fully turbulent part of the flow.

Despite the inevitably high computational cost, there has been a large effort in academic circles over the past 40 years at developing models of turbulence that are applicable in both the fully turbulent regime and the viscous sub-layer—so-called low-Reynolds-number models. Models of this type range from the simple mixing-length schemes from the 1960s and two-equation eddy viscosity models (EVMs) from the 1970s through to more intricate connections between the turbulent fluxes and the mean-field gradients, exemplified by non-linear eddy-viscosity models (NLEVMs) and second-moment closures.

While such low-Reynolds-number models have enabled accurate CFD computations to be made of a range of difficult flows, they are not the subject of this review (although results obtained with some will be included in later comparisons). Instead, attention is directed at much simpler approaches to handling the sub-layer region known as wall functions (Patankar and Spalding, 1967). Wall functions can be of many different types; their aim, however, is to replace the difference equations solved on a very fine grid across the sub-layer by algebraic formulae or other low-cost routes that provide the overall resistance of the region to heat and momentum transport.

Wall-function strategies are certainly the approach preferred by commercial CFD code vendors and their clients. However, the accuracy returned by many schemes when applied to new types of problems can be quite poor. As an illustration, Fig. 1 shows the computed heat-transfer coefficients produced by a range of different computors for the problem of convective heat transfer downstream from an abrupt pipe enlargement. Evidently, there are vastly different predicted variations of Nusselt number among the entries. While the example is not a recent one, the wall functions used and misused in those computations are still, for the most part, those in use today. It is thus timely that a reappraisal of practices should be undertaken.

The recommended new approaches, summarized in Section 3, are especially suitable for predicting large-scale complex flows such as arise in the internal environment of buildings, auditoria and stadia: flows to whose prediction Professor Shuzo Murakami, one of the dedicatees of this issue, has made such a large contribution.
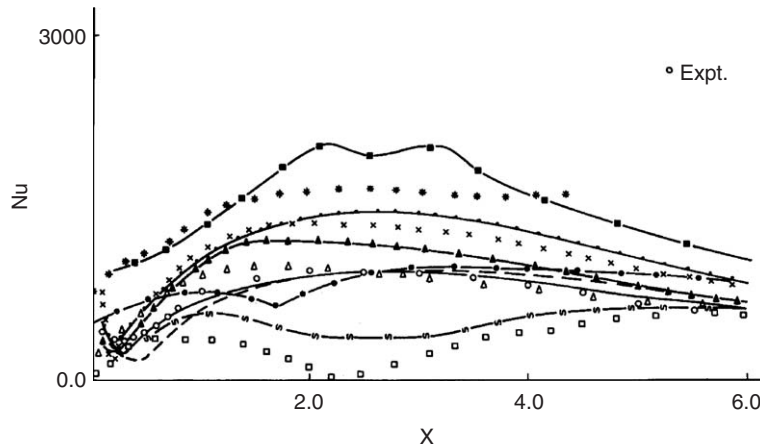
Fig. 1. Nusselt number distributions downstream of an abrupt pipe enlargement submitted for an IAHR Workshop, 1987 (Personal communication, A.G. Hutton and R. Szczepura).

2. Essential features of the VSL and simple approaches to its modelling

Imagine a wall whose surface lies in the x–z plane with the mean velocity, U, in the x direction. At the wall itself, the no-slip condition requires that the fluctuating velocity components should vanish. Moreover, if the density may locally be assumed uniform, from continuity the fluctuating velocity gradient in the direction normal to the wall, y, must also vanish. Thus, if the velocity components are expanded in a Taylor series in terms of the wall-normal distance, we deduce that while the normal stresses $\overline{u^2}$ and $\overline{w^2}$ initially increase as y^2, $\overline{v^2}$ increases as y^4 (throughout the article *kinematic* stresses are employed with typical dimensions $(m/s)^2$). Equally important, the turbulent shear stress $\overline{uv}$ increases only as y^3. These different exponents of dependency on y have been well confirmed both by experiment and direct numerical simulation (Fig. 2).

Because of the thinness of the sub-layer across which the changeover from molecular to turbulent transport occurs, in simple flows the shear stress parallel to the wall within the fluid is often essentially uniform and equal to the wall kinematic shear stress, τ_w/ρ. As one moves away from the wall there is a progressive switchover from molecular to turbulent stress as exemplified by the y^3 variation noted above. As Reynolds' pioneering paper (Reynolds, 1895) first showed, the rate of conversion of mean kinetic energy into turbulent kinetic energy by mean shear is equal to $-\overline{uv}\,\partial U/\partial y$. In a constant stress layer this leads directly to the conclusion (Rotta, 1962) that the maximum rate of turbulence energy generation occurs where the turbulent and viscous stresses are equal, i.e. where $v\partial U/\partial y = -\overline{uv} = \frac{1}{2}\tau_w/\rho$. That is why in simple wall shear flows the most intense turbulent velocity fluctuations normally appear within the VSL.

If the region adjacent to the wall is at constant shear stress, then dimensional analysis readily suggests that within that region

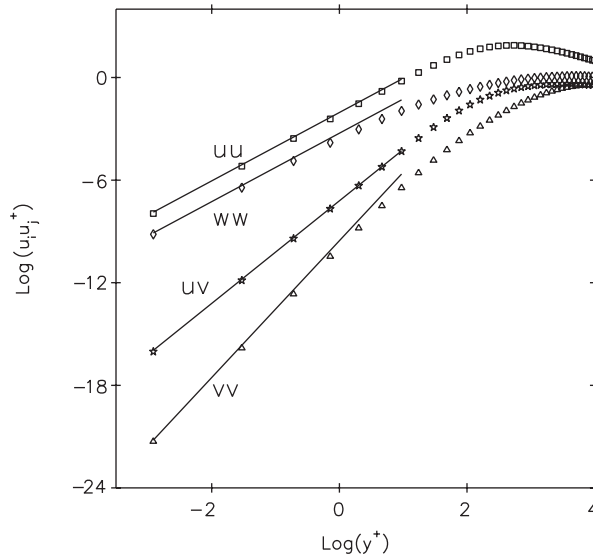$$U^+ \equiv U/U_\tau = f(y^+) \equiv f(yU_\tau/v), \tag{1}$$

Fig. 2. Near-wall variation of the Reynolds stresses. Symbols: DNS data of Kim et al. (1987); solid lines are of slope 2 (for $\overline{u^2}$ and $\overline{w^2}$), 3 (for $\overline{uv}$) and 4 (for $\overline{v^2}$).

where U_τ is the friction velocity $\sqrt{\tau_w/\rho}$. If the region of validity of Eq. (1) extends into the fully turbulent regime, various arguments, ranging from the mixing-length hypothesis to Millikan's overlap concept (Millikan, 1939), may be employed to infer that there Eq. (1) may be particularized to

$$U^+ = \frac{1}{\kappa} \ln(Ey^+), \tag{2}$$

where κ and E are regarded as universal constants. While κ, usually known as the von Karman constant, reflects the structure of turbulence in this 'fully turbulent' region, the coefficient E is dependent upon the flow structure over the VSL.

Eq. (2) is of course very well known and has been used directly for applying effective wall boundary conditions in CFD methods to avoid having to resolve the viscous sub-layer (Bradshaw et al., 1967). As such, it may be said to be the earliest 'wall function'. What is less extensively appreciated is how narrow the validity of this relationship is. The reason is that Eq. (1) (and hence Eq. (2)) is applicable only if the shear stress remains very nearly constant across the region to which it is applied. Even a decrease in shear stress across the sub-layer of just 5% causes a marked increase in the constant E in Eq. (2). Physically this amounts to a thickening, in terms of y^+, of the VSL due, ultimately, to the decline of turbulence energy generation relative to viscous dissipation in the sub-layer. Such a decrease in shear stress may arise inter alia from flow acceleration (Jones and Launder, 1972b; Perkins and McEligot, 1975; Kays and Moffat, 1975); suction through the wall (Kays and Moffat, 1975); net buoyant force on vertical walls (Jackson and Hall, 1978) or, indeed, even in fully-developed pipe flow at bulk Reynolds numbers below 10^4 (Kudva and Sesonske, 1972; Patel and Head, 1969).

Likewise, a shear stress which increases strongly with distance from the wall (whether caused by an adverse pressure gradient or transpiration through a porous wall) can lead to a thinning of the sublayer (Simpson et al., 1969; Spalart and Leonard, 1986; Launder, 1986). The picture is further complicated by

flow impingement where turbulence energy is generated by the interaction of normal stresses and normal strains rather than by shear.

The thermal equivalent to Eq. (2) is

$$\Theta^+ = \frac{1}{\tilde{\kappa}} \ln(\tilde{E} y^+), \tag{3}$$

where Θ^+ is the dimensionless temperature difference $(\Theta_w - \Theta)\rho U_\tau C_p / \dot{q}''_w$, the quantity $\dot{q}''_w$ is the wall heat-flux, and $\tilde{\kappa}$ and $\tilde{E}$ are the thermal counterparts of κ and E. Note, however, that $\tilde{E}$ depends on the Prandtl number of the fluid, σ. By introducing Eq. (2), Eq. (3) may be re-written as

$$\Theta^+ = \frac{\kappa}{\tilde{\kappa}} \left[U^+ + \frac{1}{\kappa} \ln(\tilde{E}/E) \right]. \tag{4}$$

The ratio $\kappa/\tilde{\kappa}$ is essentially what is referred to as the *turbulent Prandtl number*, σ_t, and the result may thus be re-cast as

$$\Theta^+ = \sigma_t \left(U^+ + P \left(\frac{\sigma}{\sigma_t} \right) \right). \tag{5}$$

The quantity P (usually termed the Jayatilleke pee-function) can be determined from experimental data (Jayatilleke, 1969) or from analysis, assuming a distribution of turbulent viscosity and turbulent Prandtl number over the viscous region, (Spalding, 1967b; Patankar and Spalding, 1967).

A particularly simple form (Spalding, 1967b)

$$P \equiv 9.24 \left\{ \left(\frac{\sigma}{\sigma_t} \right)^{3/4} - \left(\frac{\sigma}{\sigma_t} \right)^{1/4} \right\} \tag{6}$$

has been widely adopted. As suggested by Eq. (6), P provides a measure of the different 'resistances' of the sub-layer to heat and momentum transport; when σ is less than σ_t, P is negative.

While, as noted above, the presumption that the viscous sub-layer is of universal (dimensionless) thickness renders the formulae discussed above of limited applicability even in simple shear flow, more serious weaknesses appear in situations where the near-wall flow ceases to be shear dominated; for example, at separation or stagnation points. Then the use of the friction velocity, U_τ, as the normalizing velocity scale leads to absurd results such as a zero heat transfer coefficient at a stagnation point! This weakness was partly removed (Spalding, 1967a; Gosman et al., 1969) by replacing U_τ in the quantities appearing in Eq. (2) by $c_\mu^{1/4} k_r^{1/2}$, where k_r denotes the turbulent kinetic energy at some reference near-wall point in the fully turbulent region and c_μ is a constant (usually taken as 0.09). Thus, the conventional forms of Eqs. (2) and (3) are generalized to

$$U^* = \frac{1}{\kappa^*} \ln(E y^*), \quad \Theta^* = \sigma_t(U^* + P^*), \tag{7}$$

where

$$U^* \equiv \rho U k_r^{1/2}/\tau_w, \quad \Theta^* \equiv (\Theta_w - \Theta)\rho C_p k_r^{1/2}/\dot{q}''_w, \quad y^* \equiv \rho y k_r^{1/2}/\mu \tag{8}$$

and $\kappa^* \equiv c_\mu^{1/4}\kappa$, $E^* \equiv c_\mu^{-1/4}E$, $P^* \equiv c_\mu^{-1/4}P$.

Wall functions also need to be provided for any turbulence variables computed during the course of the computations, most usually for the turbulence energy, k, and its dissipation rate, ε. When turbulence in the fully turbulent near-wall region is in equilibrium, we may assume locally that the production and dissipation of turbulence energy are in balance. Thus for simple shear

$$\varepsilon = -\overline{uv}\,\frac{\partial U}{\partial y}. \tag{9}$$

This prescription is often used to fix the value of ε at the near-wall node in boundary-layer (marching) solvers where the flow next to the wall is, indeed, often close to local equilibrium. The turbulent kinetic energy in these circumstances is likewise prescribed in terms of the wall shear stress as

$$k = c_\mu^{-1/2}\tau_{\mathrm{w}}/\rho. \tag{10}$$

In separated flows, where local generation rates and the wall shear stress may be close to zero even though the near wall turbulence energy may be large, these practices are inadequate. This includes many situations where heat-transfer rates are of interest. Here the practice usually followed is to solve the budget equation for k, assuming zero diffusion of turbulence energy to the wall (which is reasonable since k varies as y^2 at the wall and its transport is driven by molecular diffusion). The most complete statement of this approach is given by Chieng and Launder (1980). A crucial element in the procedure lies in deciding the average generation and dissipation rates of k over the near-wall-cell, since the variation of each is highly non-linear. For a cell extending to a height y_n from the wall, the average generation rate of turbulence energy, presuming the generation arises simply from shearing, is

$$\overline{P} = -\frac{1}{y_n}\int_0^{y_n}\overline{uv}\,\frac{\mathrm{d}U}{\mathrm{d}y}\,\mathrm{d}y. \tag{11}$$

Too often, in the above, $(-\overline{uv})$ is replaced by τ_{w}/ρ which leads to the attractively simple but incorrect result

$$\overline{P} = \frac{\tau_{\mathrm{w}}U_n}{\rho y_n}. \tag{12}$$

The problem with the above is that within the truly viscous sub-layer the shear stress is transmitted by molecular interactions, not by turbulence, and there is no creation of turbulence linked with the (usually) intense velocity gradient there. What one should instead have is

$$\overline{P} = \frac{\tau_{\mathrm{w}}(U_n - U_v)}{\rho y_n}, \tag{13}$$

which is based on the simple notion that there is an abrupt changeover from molecular to turbulent transport at a distance y_v from the wall. A corresponding strategy is applied to obtain the mean energy dissipation rate, $\bar{\varepsilon}$. In this case (as detailed in Section 3) within the sub-layer, the local dissipation rate is not zero. Indeed, DNS studies of near-wall turbulence usually show that the maximum value occurs at the wall itself. The first attempt to incorporate dissipation in the viscous sublayer into a wall-function treatment appeared in Chieng and Launder (1980). However, it was found that, typically, the level of *Nu* in separated flows was underestimated by 20–30%. Reasonable accord with experiment was achieved, however, by allowing the sub-layer to become thinner when there was substantial diffusion of turbulent

kinetic energy towards the wall, broadly in line with earlier experimental observations noted above (Johnson and Launder, 1982).

Amano (1984) developed a more elaborate wall-function treatment by decomposing the viscosity-affected zone into a laminar sub-layer and a buffer region where turbulent transport is increasingly important as one proceeded away from the wall. Another significant difference was his practice of determining the near-wall value of $\bar{\varepsilon}$ from its transport equation rather than by prescribing the length scale. He examined similar pipe-expansion test flows to Johnson and Launder (1982) but concluded that his two-layer viscous/buffer model gave satisfactory agreement with experiment, whereas the Chieng–Launder single-layer version produced too *high* values of *Nu* even though, in representing the velocity field, he adhered to a constant dimensionless sub-layer thickness. The reason for this strikingly different behaviour from that reported by Johnson and Launder (1982) was probably linked with the necessarily crude, coarse-grid approximation of the source-terms in the ε-equation over the near-wall cell.

Finally, Ciofalo and Collins (1989) confirmed the conclusion of Johnson and Launder (1982) that the variation of the sub-layer thickness is, indeed, a vital element of any wall treatment for impinging or separated flows. However, they related the sub-layer thickness not to the diffusive inflow (or outflow) of turbulence energy but to the local turbulence intensity, $k^{1/2}/U$, at the near-wall node, a practice that, from a numerical point of view, was certainly more stable.

3. Two current wall-function approaches

For at least 10 years preceding the work summarized below there seems to have been little, if any, work directed at improving wall-function practices, at least within the context of RANS computations. The available schemes were, however, plainly deficient on various counts.

At UMIST, two projects have been focused on developing more general wall-functions. Each has adopted a quite different pathway: one is an analytical scheme, UMIST—A (Unified Methodology for Integrated Sub-layer Transport—Analytical), the other numerical (UMIST—N). While the latter scheme is the more general, the former is more evidently an evolution of the practices reported in Section 2. In the following sections, a brief account of both schemes is provided, with examples of their applications.

All the computations have been performed with suitably adapted versions of the TEAM computer code (Huang and Leschziner, 1983), which is a finite-volume based solver, employing a Cartesian grid with fully staggered storage arrangement and the SIMPLE pressure correction scheme of Patankar (1980). For most of the calculations the QUICK scheme of Leonard (1979) has been used for convection of the mean variables, with PLDS of Patankar (1980) applied for the turbulence quantities. In all cases grid refinement studies have shown that the results presented are free from numerical discretization errors.

3.1. UMIST—A Scheme

The UMIST—A scheme provides a clear, albeit simple, physical model based on an analytical solution of the streamwise momentum and energy equations in the near-wall region. It was commissioned for use in safety studies by a consortium of UK nuclear-power companies who were concerned that available wall functions did not permit a realistic representation of the near-wall flow under mixed or natural-
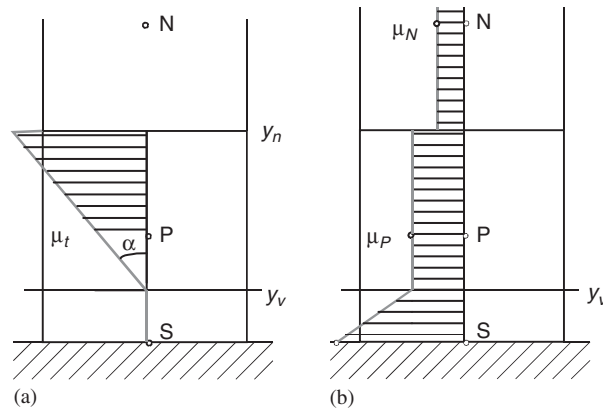
Fig. 3. Viscosity distributions assumed over near-wall cell. (a) Turbulent viscosity. (b) Molecular viscosity.

convection conditions such as may arise following a failure of the reactor circulation pumps. Specifically the approach has been designed to be able to cope with

- forced, mixed or natural convection flow on near vertical surfaces,
- strong variations of molecular transport properties across the VSL,
- laminarization, i.e. a marked thickening of the VSL in buoyancy-aided mixed convection.

A detailed account of the resultant scheme has been published (Craft et al., 2002) while a comprehensive description may be found in the PhD thesis of Gerasimov (2003). Here just the main elements that especially relate to the above capabilities are noted. The starting point is a prescribed ramp distribution of turbulent viscosity (Fig. 3(a)),

$$\frac{\mu_t}{\mu_v} = c_\mu c_l (y^* - y_v^*) \quad \text{for } y^* \geqslant y_v^*. \tag{14}$$

The coefficients c_μ and c_l are the conventional ones adopted in 1-equation turbulence models (0.09, 2.55) where now $y^* \equiv \rho_v y k_P^{1/2} / \mu_v$ and the subscript denotes where the quantity is evaluated: 'v'— at the edge of the viscous layer; 'P'— at the near-wall node. This rather simple viscosity profile is essential to retain a form of the near-wall differential equations that can be analytically integrated to give velocity and temperature profiles. One important aspect of this integration is that source terms in the streamwise momentum equation representing pressure gradients or buoyancy can be retained. The subsequent profiles are then used to obtain quantities such as wall shear stress and cell-averaged source terms which are required for the wall function treatment.

Initially it was intended to evaluate k in the definition of y^* at the sub-layer interface, y_v, as proposed in Chieng and Launder (1980). However, this proved a much less stable practice than adopting the nodal value and, surprisingly, it also led to greater dependence on the size of the near-wall cell. (The reason being that to extrapolate values to y_v requires the use of information further from the wall than y_P).

In flows with intense wall heating some account of the variation of molecular properties across the sub-layer due to temperature changes also needs to be taken, Fig. 3(b). The function introduced for the variation of μ needs to be simple enough to allow the momentum equation to be integrated across the
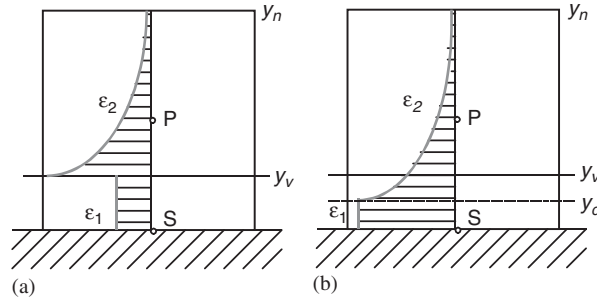
Fig. 4. Distribution of ε over near-wall cell. (a) Conventional prescription (Chieng and Launder, 1980). (b) Currently adopted variation.

sub-layer, and it was found that the exact form adopted can profoundly affect the numerical stability of the equation set. To allow the analytical integration to be carried out, it was first found preferable to cast the dependence in terms of y^* rather than of temperature (with the function chosen providing an interpolation between the values of viscosity at the wall and at y_v). Secondly, although a linear variation was initially tried, this turned out to be much less stable than a hyperbolic variation:

$$\mu = \mu_v/[1 + b_\mu(y^* - y_v^*)] \quad \text{for } 0 < y^* < y_v^*, \tag{15}$$

where $b_\mu = (\mu_{\text{wall}} - \mu_v)/(y_v^*\mu_{\text{wall}})$.

Another area where it was felt appropriate to improve current practice was in the prescription of the kinetic energy dissipation rate next to the wall, Fig. 4. Chieng and Launder (1980) had approximated the exact result of Jones and Launder (1972a),

$$\varepsilon_v = v\left(\frac{\partial k^{1/2}}{\partial y}\right)^2 \approx \frac{2vk}{y^2} = \frac{2vk_P}{y_v^2}. \tag{16}$$

However, while k varies parabolically with y very close to the wall, it levels out near the point of maximum k-production. Consequently, the last form in Eq. (16) gives sub-layer dissipation levels lower than those in the adjacent fully-turbulent zone, a result which is at odds with all DNS data. To correct this anomaly it was supposed that the sub-layer for the dissipation rate was smaller than y_v, the distance being chosen so that the dissipation rates in the two zones were equal at $y = y_d$,

$$\varepsilon_{\text{w}} = 2vk_P/y_d^2 = k_P^{3/2}/(c_l y_d). \tag{17}$$

In fact, the choice of smaller y_d than y_v has been made in a number of the low-Reynolds-number turbulence models (Wolfshtein, 1969). The mean value of ε over the inner cell is then obtained by integration over the near-wall control volume as in Chieng and Launder (1980) and Ciofalo and Collins (1989).

To make the treatment sensitive to laminarization two choices had to be made, namely appropriate parameters to use as *detector* and *operand*. After extensive testing, we concluded, in line with some of the earlier mixing-length models, that the ratio of the shear stress between the wall and the edge of the sub-layer, λ, was the best detector. Initially we attempted to correlate y_v^* as a function of this parameter but this proved to have poor stability characteristics. Accordingly, a more direct choice for the operand
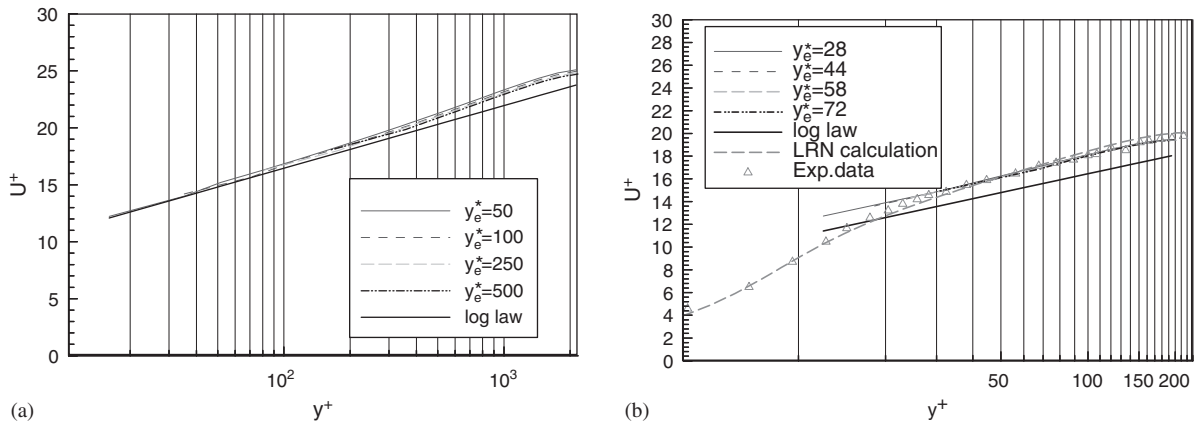
Fig. 5. Mean velocity profile in pipe flow in wall-layer coordinates. (a) $Re = 10^5$. (b) $Re = 6753$. Symbols: experiments of Kudva and Sesonske (1972); solid line: log-law; light broken line: LRN calculation; other lines: UMIST—A with different near-wall cell sizes.

was adopted: the mean level of dissipation rate over the near-wall control volume (obtained as noted in the preceding paragraph) was adjusted by a weighting function F that in turn was a function of λ as

$$\bar{\varepsilon}_{\text{new}} = F(\lambda)\bar{\varepsilon}_{\text{old}}. \tag{18}$$

Other features of the overall scheme to note are that:

- Convective transport (which is ignored in many wall-function treatments) is retained in simplified form.
- When buoyancy is important, the buoyant force in the discretized vertical momentum equation in the near-wall cell is obtained by integrating a fit to the analytical temperature profile over the cell rather than basing the force purely on the temperature at the near-wall node itself.
- When the viscous sub-layer thickness exceeds the cell thickness, y_n (as it may do in limited regions if a structured grid is adopted), a reformulation is needed, but the analysis can still be carried out based on identical principles.

These and other features of the scheme are detailed by Craft et al. (2002).

Figs. 5–10 provide an impression of the capabilities of the method. Fig. 5 shows the variation of velocity on wall-law axes for two fully-developed pipe flows. At a Reynolds number of 10^5 the scheme is seen to return results which do lie on the log-law. However, at a lower Reynolds number of 6753 the experimental data of Kudva and Sesonske (1972) lie above the supposedly 'universal' log-law, as do predictions with the low-Reynolds-number (LRN) k–ε model of Launder and Sharma (1974). More importantly, the present wall-function results also accord with the data. In contrast to most such schemes, it should also be noted that the UMIST—A scheme results show scarcely any sensitivity to the size of the near-wall cell.

As a second example, Fig. 6 relates to upflow in a vertical pipe where, at $x/d = 50$ (after 50 diameters of isothermal flow development), strong uniform heating is applied at the wall causing a buoyant upthrust on the near-wall fluid which thus accelerates. This causes a marked drop in Nusselt number below the Dittus–Boelter correlation, shown by the solid horizontal line. Again, the wall-function results accord
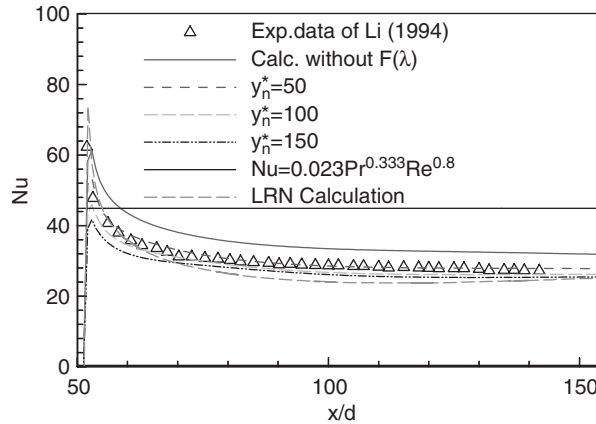
Fig. 6. Variation of Nusselt number in mixed-convection upflow in a vertical tube. Symbols: experiments of Li (1994); solid line: Dittus–Boelter; medium broken line: LRN calculation; dotted line: UMIST—A without $F(\lambda)$; other lines: full UMIST—A treatment.
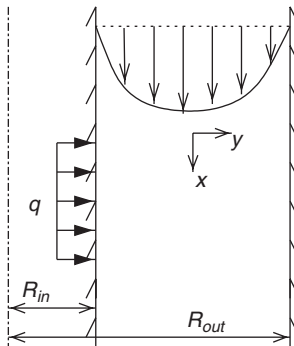

Fig. 7. Geometry of the downward flow through an annular passage.

well with the data. For one run the $F(\lambda)$ correction of Eq. (18) was not applied and this evidently leads to a 20% increase in Nusselt number. The complementary case of buoyancy opposed flow is shown schematically in Fig. 7 for downward flow through an annular passage, with inner and outer radii R_{in} and R_{out}, respectively, where a section of the core tube is heated. In this case the buoyancy leads to an increase in heat transfer levels above what would be found in pure forced convection. As seen in Fig. 8, at a fairly low level of buoyancy the full low-Reynolds-number model of Launder and Sharma (1974) and both wall function treatments broadly capture the small increase in Nusselt number (for comparison the graphs also show the results returned by the low-Reynolds-number scheme for the equivalent forced convection flow). However, at higher values of the buoyancy parameter, Fig. 9 shows that both the UMIST—A scheme and the full low-Reynolds-number do capture the now substantial increase in Nusselt number found in the experiments, whereas the standard wall functions described in Section 2 do not.

Sometimes, of course, one needs a more elaborate description in the main part of the flow than the 2-equation eddy-viscosity model of the preceding examples: flows with complex strains or other major
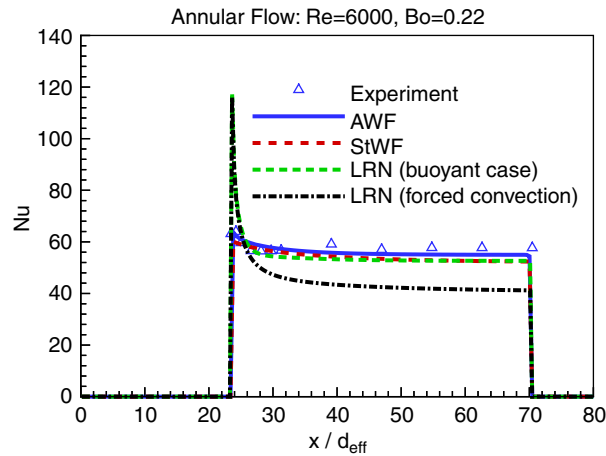
Fig. 8. Nusselt number variation along a heated annulus wall at a low buoyancy parameter Bo = 0.22. Symbols: experiments of Jackson et al. (2002); LRN: low-*Re* model calculations; StWF: standard wall function predictions; AWF: UMIST—A predictions.
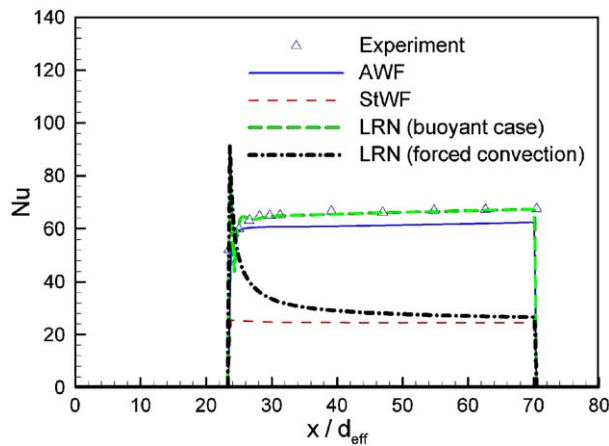

Fig. 9. Same as Fig. 8, but for Bo = 2.89.

departures from the simply sheared local-equilibrium structure for which a linear eddy-viscosity model is most suited. Fig. 10 shows a downward-directed wall jet with a weak opposing, upward-moving stream. The flow relates to safety studies in a nuclear reactor with the crucial item to predict accurately being the depth of penetration of the wall jet. We note that in this case, while the UMIST—A scheme used with the *k–ε* EVM mimics the low-*Re* *k–ε* model with the same fidelity as before, because of the more complex strain field in this case neither is in close accord with the LES results of Addad et al. (2003). When the external flow is computed with a second-moment closure (where one solves transport equations for all the turbulent stresses) agreement with the LES results is much improved, however. The level of agreement depends on the particular second-moment closure used. The 'TCL' results in Fig. 10 refer to our preferred scheme that satisfies all kinematic constraints on the turbulent stresses in the two-component limit (Craft et al., 1996a).
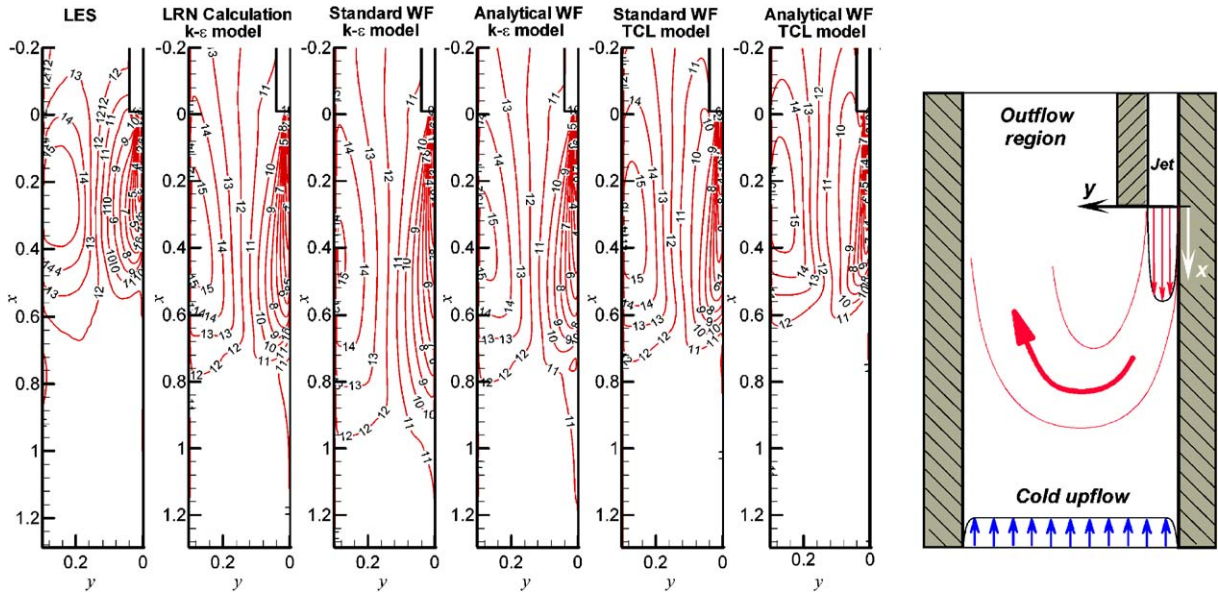
Fig. 10. Vertical velocity contours in the opposed wall jet flow. LES of Addad et al. (2003); k–ε calculations with low-Re-number near wall treatment, standard and UMIST—A wall functions; TCL stress transport model predictions with standard and UMIST—A wall functions.

3.2. UMIST—N scheme

One type of flow for which the above analytical approach is not well equipped is where the velocity profile parallel with the wall undergoes strong skewing across the sublayer, as it does, for example, in the oblique impingement of flow on a bank of heat-exchanger tubes. Moreover, for flow with strong streamline curvature, it is known that the linear stress–strain relation adopted in eddy-viscosity models does not adequately mimic the turbulence-generation processes. In view of the above difficulties, a different strategy has been evolved, UMIST—N (Gant, 2002; Craft et al., 2004). In form it is much more akin to low-Reynolds-number models in that the wall-function cell is itself sub-divided into, typically, 30 thin slices, Fig. 11. The mean flow and turbulence differential equations, with suitable simplifications, are solved effectively as a one-dimensional problem across this fine grid in order to generate the data required as 'wall-function' quantities (wall shear stress, averaged source terms, etc.) to supply appropriate wall boundary conditions for the whole-field solution carried out on the primary grid.

Of course, as noted, simplifications are made to the equations solved on the fine grid in order to secure the great reduction in computer time that one seeks from wall functions. Firstly, the pressure gradient parallel to the wall is assumed uniform across all the sub-grids, equal to the pressure gradient across the near-wall cell of the primary grid. Moreover, the velocity component normal to the wall is found by continuity rather than by solving the momentum equation normal to the wall. In these respects the fine-grid solution is essentially obtained with a separate boundary-layer solver. It is, however, applied simply to the immediate near-wall layer extending to values of y^* of 100 or less. Boundary conditions imposed at the outer edge of the subgrid at $y = y_n$ are simply interpolated from values held on the primary grid at y_P and y_N. At the wall itself the same boundary conditions are applied as for
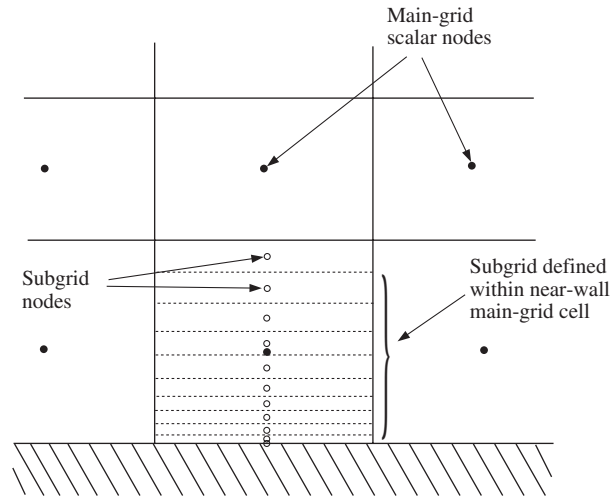
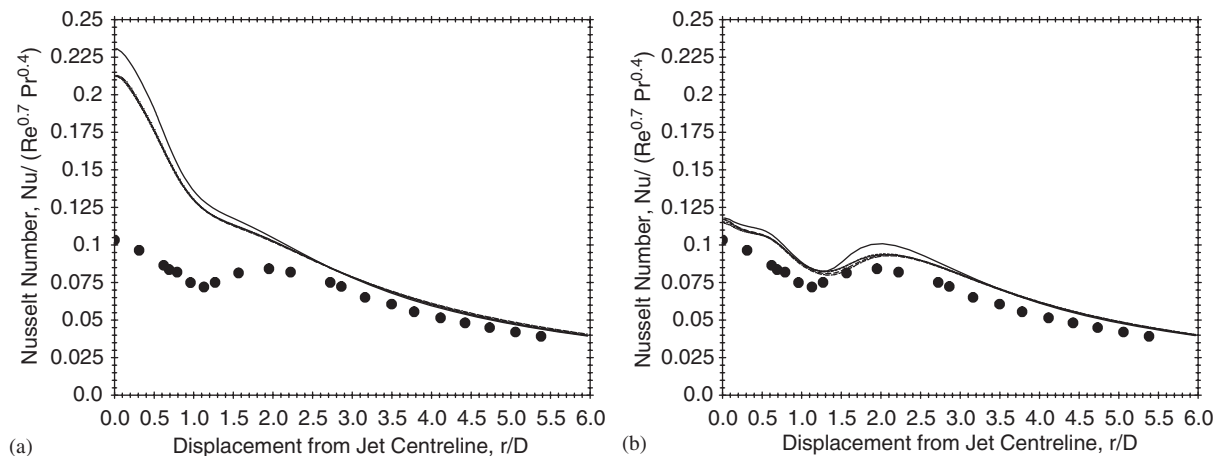Fig. 11. Treatment of near-wall control volume in UMIST—N.

Fig. 12. Nusselt number variation on a flat plate beneath an axisymmetric impinging jet. (a) Linear k–ε EVM. (b) Cubic non-linear EVM (Craft et al., 1996b). Symbols: experiments of Baughn et al. (1992); heavy line: full LRN treatment; other lines: UMIST—N, with different near-wall cell sizes.

a conventional treatment of a LRN model, including zero values for the mean velocity components and k.

Two alternative turbulence models have been employed within the above numerical treatment: the LRN k–ε model of Launder and Sharma (1974) and a cubic non-linear eddy viscosity model of Craft et al. (1996b). The cubic terms in the latter model make it far more sensitive to streamline curvature than a linear EVM. The first test case is for a turbulent jet impinging orthogonally onto a flat, uniformly heated plate. The jet discharges from a long smooth pipe whose exit is four diameters above the plate. Fig. 12 shows the resultant variation of Nusselt number over the plate from the stagnation point ($r = 0$) outwards. In fact,
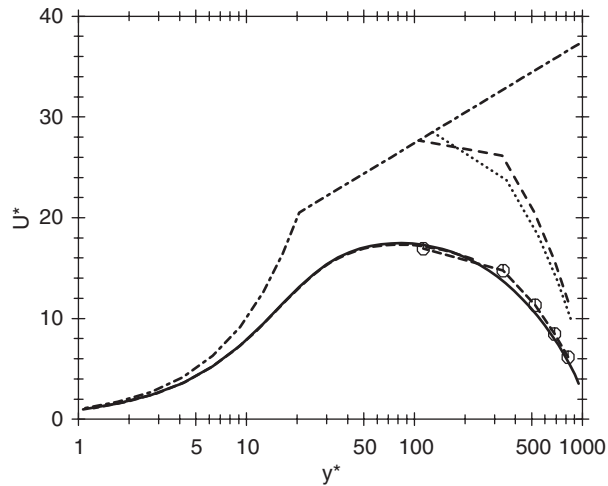
Fig. 13. Radial velocity profile for spinning disc in wall-layer coordinates. Solid line: LRN calculation; broken line with symbols: UMIST—N; chain line: log-law; other lines: standard wall-function treatments.

linear eddy viscosity models do a poor job at reproducing impinging flows because of the very different strain field than is found in simple shear. As is seen in Fig. 12(a), the computed Nusselt number at the stagnation point is more than twice the measured value. However, at least the wall-function solutions are in close accord with the complete LRN computations: in other words the much simplified treatment over the near-wall cell has had only a very minor effect on the computed Nusselt number. Fig. 12(b) presents results for the same test flow but where the non-linear EVM (Craft et al., 1996b) is adopted. Agreement with experiment is now much closer and, as with the linear EVM, there is close accord between the wall-function and complete LRN treatments. Note too that there is scarcely any sensitivity to the thickness of the 'wall-function' region, which is a very desirable characteristic. The only major difference between the UMIST—N results and those of the complete LRN treatment is in the computer time required: the wall-function result with the same grid density takes less than one eighth of the time required for the complete low-Reynolds-number model.

As a final example we consider heat transfer from a mildly heated disc spinning about its own axis. The disc's rotation induces a radially outward motion that peaks outside the VSL. The tangential velocity, by contrast, increases rapidly across the sublayer to Ωr on the disc surface (Ω the disc's angular velocity and r the local radius). Hence, the mean velocity vector undergoes severe skewing across the VSL. This effect is satisfactorily reproduced by virtually any LRN model but cannot be accounted for with conventional wall functions (including UMIST—A) which, with the wall-adjacent node in the turbulent region, incorrectly take the wall shear stress to point in the same direction as the near-wall velocity vector. Fig. 13, however, shows that the induced radial velocity predicted with the numerical wall function (using the linear EVM of Launder and Sharma, 1974) agrees very closely with the results of the corresponding LRN computation. The integral Nusselt number in Fig. 14 also shows negligible differences among the alternative treatments: all the computations reproduce the experimental data with reasonable fidelity. In this case, for equivalent grids and convergence limits, the complete low-Reynolds-number model required thirteen times more computation time than UMIST—N!
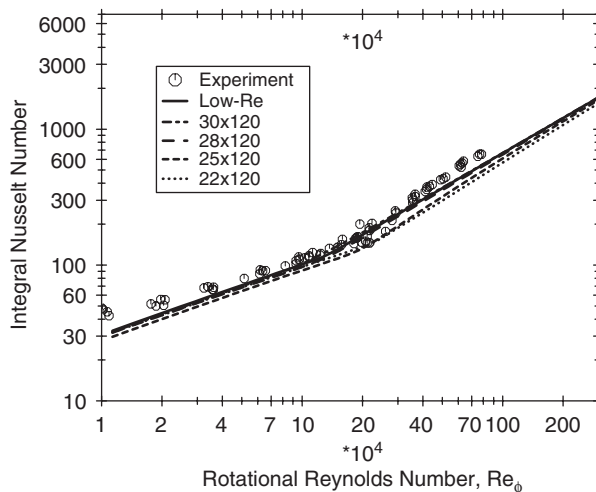
Fig. 14. Variation of Nusselt number for spinning disc with Reynolds number. Symbols: experiment of Cobb and Saunders (1956); heavy line: Full LRN treatment; other lines: UMIST—N.

4. Conclusions

Two new wall-function approaches have been presented. The first is based on the analytical solution of simplified near-wall momentum and temperature equations, accounting for pressure gradients and other force fields such as buoyancy, whilst the second is based on a local one-dimensional numerical solution of the governing equations. Both approaches have been applied to a range of flows in which standard log-law based wall functions are known to perform badly. In each case the present methods have been shown to mimic the results obtainable with full low-Reynolds-number solutions, but at a fraction of the computational cost. Whilst both proposed schemes undoubtedly have their own advantages and disadvantages, much wider testing will be required before any definitive statement can be given on the superiority of one approach over the other. UMIST—N is, in principle, the more general approach, but is inevitably more computationally expensive than UMIST—A (both in terms of cpu time and storage requirements). The overall methodology of UMIST—A, on the other hand, is closer to that employed in standard wall-functions, thus possibly making it the easier scheme to incorporate into existing flow solvers.

As a final observation on both the wall-function approaches outlined in this section, all the applications so far considered are relatively straightforward compared with the types of flows the industrial user needs to compute. However, we see no evident impediment to their use in these more complex flows. Indeed, we hope that the turbulent-flow CFD community will contribute to this wider testing and, where necessary, the improvement of these prototype forms.

Acknowledgements

to acquire both a detailed appreciation of the research of all three as well as a close, enduring personal relationship.

The research summarized in Section 3 has been supported by British Energy, plc and the UK Engineering and Physical Sciences Research Council.

References

Addad, Y., Laurence, D., Benhamadouche, S., 2003. The negatively buoyant wall-jet. part 1: LES database. In: Proceedings of fourth International Symposium on Turbulence Heat and Mass Transfer. Antalya, Turkey.

Amano, R., 1984. Development of a turbulence near-wall model and its application to separated and reattached flows. Numer. Heat Transfer 7, 59–76.

Baughn, J.W., Yan, X., Mesbah, M., 1992. The effect of Reynolds number on the heat transfer distribution from a flat plate to an impinging jet. In: ASME Winter Annual Meeting.

Bradshaw, P., Ferriss, D.H., Attwell, N.P., 1967. J. Fluid Mech. 29, 625.

Chieng, C.C., Launder, B.E., 1980. On the calculation of turbulent heat transport downstream from an abrupt pipe expansion. Numer. Heat Transfer 3, 189–207.

Ciofalo, M., Collins, M.W., 1989. k–ε predictions of heat transfer in turbulent recirculating flows using an improved wall treatment. Numer. Heat Transfer 15, 21–47.

Cobb, E.C., Saunders, O.A., 1956. Heat transfer from a rotating disk. Proc. R. Soc. London A 236, 343–351.

Craft, T.J., Ince, N.Z., Launder, B.E., 1996a. Recent developments in second-moment closure for buoyancy-affected flows. Dyn. Atmo. Oceans 23, 99–114.

Craft, T.J., Launder, B.E., Suga, K., 1996b. Development and application of a cubic eddy-viscosity model of turbulence. Int. J. Heat Fluid Flow 17, 108–115.

Craft, T.J., Gerasimov, A.V., Iacovides, H., Launder, B.E., 2002. Progress in the generalization of wall-function treatments. Int. J. Heat Fluid Flow 23, 148–160.

Craft, T.J., Gant, S.E., Iacovides, H., Launder, B.E., 2004. A new wall function strategy for complex turbulent flows. Numer. Heat Transfer 45, 301–318.

Gant, S.E., 2002. Development and application of a new wall function for complex turbulent flows. Ph.D. Thesis, Department of Mechanical, Aerospace & Manufacturing Engineering, UMIST, Manchester.

Gerasimov, A.V., 2003. Development and application of an analytical wall-function strategy for modelling forced, mixed and natural convection flows. Ph.D. Thesis, Department of Mechanical, Aerospace & Manufacturing Engineering, UMIST, Manchester.

Gosman, A.D., Pun, W.M., Runchal, A.K., Spalding, D.B., Wolfshtein, M., 1969. Heat and Mass Transfer in Recirculating Flows. Academic Press, London.

Huang, P.G., Leschziner, M.A., 1983. An introduction and guide to the computer code TEAM. Technical Report TFD/83/9(R), Mechanical Engineering Department, UMIST.

Jackson, J.D., Hall, W.B., 1978. Forced convection heat transfer to supercritical-pressure fluids. In: NATO Advanced Studies Institute. Bogazia University, Istanbul.

Jackson, J.D., He, S., Xu, Z., Wu, T., 2002. CFD quality and trust: generic studies of thermal convection. Technical Report HTH/GNSR/5029, University of Manchester.

Jayatilleke, C.L.V., 1969. The influence of Prandtl number and surface roughness on the resistance of the laminar sublayer to momentum and heat transfer. Prog. Heat Mass Transfer 1, 193.

Johnson, R.W., Launder, B.E., 1982. Discussion of 'On the calculation of turbulent heat transport downstream from an abrupt pipe expansion'. Numer. Heat Transfer 5, 493–496.

Jones, W.P., Launder, B.E., 1972a. The prediction of laminarization with a two-equation model of turbulence. Int. J. Heat Mass Transfer 15, 301–314.

Jones, W.P., Launder, B.E., 1972b. Some properties of sink-flow turbulent boundary layers. J. Fluid Mech. 56, 337–351.

Kays, W.M., Moffat, R.J., 1975. Studies in convection, vol. 1. Academic Press, New York.

Kim, J., Moin, P., Moser, R., 1987. Turbulence statistics in fully developed channel flow at low Reynolds number. J. Fluid Mech. 177, 133–166.

Kudva, A.A., Sesonske, A., 1972. Structure of turbulent velocity and temperature fields in ethylene glycol pipe flow at low Reynolds number. Int. J. Heat Mass Transfer 15, 127.

Launder, B.E., 1986. Low-Reynolds-number turbulence near walls. Technical Report TFD/86/4, Department of Mechanical Engineering, UMIST.

Launder, B.E., Sharma, B.I., 1974. Application of the energy-dissipation model of turbulence to the calculation of flow near a spinning disc. Lett. Heat Mass Transfer 1, 131–138.

Leonard, B.P., 1979. A stable and accurate convective modelling procedure based on quadratic upstream interpolation. Comput. Meth. Appl. Engng. 19, 59–98.

Li, J., 1994. Studies of buoyancy-influenced convective heat transfer to air in a vertical tube. Ph.D. Thesis, University of Manchester.

Millikan, C.B., 1939. A critical discussion of turbulent flows in channels and circular tubes. In: Proceedings of fifth International Congress for Applied Mechanics, pp. 386–392.

Patankar, S.V., 1980. Numerical Heat Transfer. McGraw-Hill, New York.

Patankar, S.V., Spalding, D.B., 1967. Heat and Mass Transfer in Boundary Layers. first ed. Morgan Grampian Press,

Patel, V.C., Head, M.R., 1969. Some observations on skin friction and velocity profiles in fully developed pipe and channel flows. J. Fluid Mech. 38, 181.

Perkins, K.R., McEligot, D.M., 1975. ASME J. Heat Trans. 97, 589.

Reynolds, O., 1895. On the dynamical theory of incompressible viscous fluids and the determination of the criterion. Phil. Trans. R. Soc. A 186, 123–164.

Rotta, J.C., 1962. Turbulent boundary layers in incompressible flow. In: Kuchemann, D. (Ed.), Progress in the Aeronautical Sciences, vol. 2, pp. 1–219.

Simpson, R.L., Kays, W.M., Moffat, R.J., 1969. Technical Report HMT-2, Mech. Eng. Dept., Stanford University.

Spalart, P., Leonard, A., 1986. Direct numerical simulation of equilibrium turbulent boundary layers. In: F.J.Durst et al. (Eds.), Turbulent Shear Flows—vol. 5. Springer, Heidelberg.

Spalding, D.B., 1967a. Heat transfer from turbulent separated flows. J. Fluid Mech. 27, 97.

Spalding, D.B., 1967b. Monograph on turbulent boundary layers. Technical Report TWF/TN/33, Imperial College Mechanical Engineering Department (Chapter 2).

Wolfshtein, M., 1969. The velocity and temperature distribution in one-dimensional flow with turbulence augmentation and pressure gradient. Int. J. Heat Mass Transfer 12, 301–318.